EES Batteries

ROYAL SOCIETY OF CHEMISTRY

COMMUNICATION

View Article Online
View Journal | View Issue

Cite this: *EES Batteries*, 2025, **1**, 153

Received 5th November 2024,
Accepted 7th December 2024

DOI: 10.1039/d4eb00025k

rsc.li/EESBatteries

Disentangling multifactorial impacts on cathode thermochemical properties with explainable machine learning†

Yujian Sun, ‡[a,b] Xilin Xu, ‡[a,b] Luyu Gan,‡[a] Sichen Jiao, [a,b] Shuangshuang Han,[c] Yajun Zhao,[a] Yan Li,[c] Xiqian Yu, *[a,b] Jizhou Li, *[d,e] Hong Li *[a,b] and Xuejie Huang [a,b]

Thermal safety remains a critical concern in the commercialization of lithium-ion batteries (LIBs), with extensive research dedicated to understanding the thermal behaviors of cathode materials. While a wealth of thermochemical test data is available in the literature, the variability in sample conditions and experimental testing parameters complicates the identification of fundamental relationships between the intrinsic properties and thermochemical reaction characteristics of materials. This study utilizes explainable machine learning (ML) methodologies to tackle this challenge by analyzing a comprehensive database derived from published differential scanning calorimeter (DSC) testing results. By employing meticulously curated, augmented, and filtered features that characterize material properties, sample conditions, and testing parameters, we leveraged ML models to predict and validate thermochemical reaction characteristics across the chemical compositional space of layered oxide cathode materials. Through the explainability, we elucidated multidimensional relationships between input features and thermochemical reaction characteristics, revealing that material properties predominantly dictate the initiation of the reaction, while external conditions exert a greater influence on the kinetics of heat release. This approach demonstrates the effectiveness of ML in decoding complex causal factors of cathode thermochemical reaction behaviors, thereby offering valuable insights for targeted thermal optimization in battery safety design.

Broader context

Thermal safety concerns present a critical barrier to the widespread commercialization of high-energy density lithium-ion batteries. Despite extensive experimental studies and thermal testing data across diverse cathode materials, the heterogeneity in testing conditions and incomplete parameter documentation have impeded comprehensive analysis of the literature database. This study addresses this challenge through a systematic analysis of hundreds of thermal testing data points from the published literature, employing explainable machine learning to decode the complex relationships between thermal behavior characteristics and influential factors, including material properties, electrode conditions, and testing parameters. Our analysis reveals dynamic shifts in factor contributions throughout thermal reactions, suggesting the need for stage-specific thermal optimization strategies. These findings underscore the importance of standardized thermal testing protocols for establishing comprehensive databases conducive to future data-driven analyses.

Introduction

As the commercialization of lithium-ion batteries (LIBs) accelerates towards high energy density and large-scale energy storage applications, battery safety has emerged as a paramount concern for society.[1,2] The root cause of battery safety issues lies in a sequence of exothermic reactions among the battery components that are triggered by thermal abuse or other atypical usage conditions, which result in heat accumulation and ultimately battery thermal runaway.[3–5] Among these reactions, those associated with the cathode materials are widely regarded as the primary contributors to thermal runaway,[6] wherein oxygen may be liberated from charged cathodes, especially for the layered oxide cathodes, at certain temperatures, potentially initiating combustion.[3,7] Consequently,

[a]*Beijing Frontier Research Center on Clean Energy, Institute of Physics, Chinese Academy of Sciences, Beijing 100190, China. E-mail: xyu@iphy.ac.cn, hli@iphy.ac.cn*
[b]*Center of Materials Science and Optoelectronics Engineering, University of Chinese Academy of Sciences, Beijing 100049, China*
[c]*College of New Materials and Chemical Engineering, Beijing Institute of Petrochemical Technology, Beijing 102627, China*
[d]*Department of Electronic Engineering, The Chinese University of Hong Kong, Hong Kong 999077, China. E-mail: lijz@ieee.org*
[e]*CUHK Shenzhen Research Institute, Shenzhen 518057, China*
†Electronic supplementary information (ESI) available. See DOI: https://doi.org/10.1039/d4eb00025k
‡These authors contributed equally to this work.

the thermal stability of cathode materials and the thermochemical reaction dynamics between the cathode and other battery components have been extensively investigated in recent decades. Differential Scanning Calorimetry (DSC) is a widely employed analytical technique capable of recording critical parameters associated with the thermochemical reaction processes of cathode materials, including endothermic and exothermic temperatures as well as heat flow. These parameters serve as indicators of the material's thermal stability and its kinetic interactions with other substances. However, the thermochemical reaction process is influenced not only by the intrinsic physical and chemical properties of the material[8] but also by a range of factors related to sample conditions[9] (*i.e.* the composition and ratio of non-active materials in the cathode electrode, electrolyte content in test samples, *etc.*) and testing parameters[10] (*i.e.* scanning rate for the DSC test). Unfortunately, the DSC testing of cathode materials documented in the literature often lacks standardized sample preparation and testing conditions, with incomplete records of these parameters as well. This inconsistency poses significant challenges for researchers attempting to assess the thermal stability of cathode materials through a comparative analysis of DSC characteristic parameters and to quantify the impact of various factors on the thermochemical reactions occurring within these materials.

Recent advancements in machine learning (ML) have catalyzed the integration of data-driven methodologies within experimental science.[11–16] These approaches leverage ML models to uncover underlying relationships from heterogeneous experimental datasets characterized by unevenly distributed features in high-dimensional spaces, thereby surmounting the constraints imposed by stringent variable control that is typical of traditional experiments.[17] In the context of layered oxide cathode materials ($Li_{1+x}TM_{1-x}O_2$, where TM represents 3d and 4d transition metal elements), which exhibit a broad compositional space, this paradigm has demonstrated to be highly effective in elucidating critical correlations between material composition and electrochemical performance, even in the presence of experimental noise.[18,19] However, establishing high-fidelity experimental datasets from scratch is both labor-intensive and costly, leaving data scarcity to present a significant challenge for experimental data learning.[20–24] Masalkovaitė *et al.* recently demonstrated the efficacy of transfer learning in predicting complex fractional heat output data from readily accessible mass ejection data and cell manufacturing specifications. The model's ability to generalize across diverse commercial cell types with minimal additional training data underscores its potential in addressing data scarcity challenges in battery thermal analysis.[25] Despite the significance of this work, a more fundamental investigation linking intrinsic material physical and electrochemical properties to thermal stability remains conspicuously absent.

In this study, we systematically investigated experimental data of the cathode thermal behaviors in LIBs reported in the existing literature using a data-driven ML approach. We compiled nearly six hundred thermal stability data points for cathode materials, including lithium cobalt oxide ($LiCoO_2$, denoted as LCO), nickel–cobalt–manganese ternary materials ($LiNi_xCo_yMn_zO_2$, $x + y + z = 1$, denoted as NCM) and lithium-rich layered oxide (denoted as LR), extracted from DSC results in the literature. A comprehensive analysis was conducted on multiple causal features, including the material's intrinsic physical and chemical properties, electrode sample conditions, and DSC testing parameters. Our investigation primarily concentrated on the correlation between these features and thermal behaviors, characterized by critical metrics such as the onset and peak temperatures of heat release, along with the maximum heat release power. Utilizing the trained ML model, we identified the optimal composition of NCM materials concerning thermal stability by minimizing the influence of sample and testing conditions. Additionally, through the application of explainable ML techniques, we elucidated the dynamic evolution of feature contributions to thermochemical characteristics throughout the reaction process.

Results and discussion

Feature selection

The input features of our dataset, as elaborated in Table S1,† encompass potential causal factors that influence the thermochemical reaction behavior, categorized into material properties, sample conditions, and DSC testing parameters. To enhance the interpretability of the model regarding the material's intrinsic structural attributes, we expanded the feature set by incorporating statistical derivatives of electronegativity (EN), ionic radii, and ionic potential (Φ). This augmentation of features is intended to explicitly reveal structural properties to our ML model, thereby potentially improving its learning efficiency. However, recognizing that feature proliferation does not necessarily correlate with improved performance, we implemented a two-step feature selection process. This process, based on correlation coefficients and null importance metrics, was designed to eliminate unfavorable features and optimize the dataset for subsequent analysis.

The initial step of feature selection entailed the removal of redundant features that displayed significant correlations, as these can give rise to multicollinearity, resulting in unstable regression outcomes, diminished generalization capabilities, and hindered interpretability of the model. Although Pearson coefficients are commonly utilized for multicollinearity detection, their assumption of continuous and normally distributed variables does not universally apply to our dataset. Consequently, we selected Spearman coefficients, which are more suitable for identifying general monotonic relationships across varied data distributions.[26,27] Fig. 1a presents the heatmap of Spearman correlation coefficients for all evaluated feature variables, with deep red or blue data points indicating strongly positively or negatively correlated feature pairs, respectively. For instance, the Spearman coefficient between "Ni content" and "radii-TM ave. (wt.)" is −0.98, signifying a robust negative monotonic relationship. This correlation is illustrated in Fig. 1b, where the data points are aligned along a

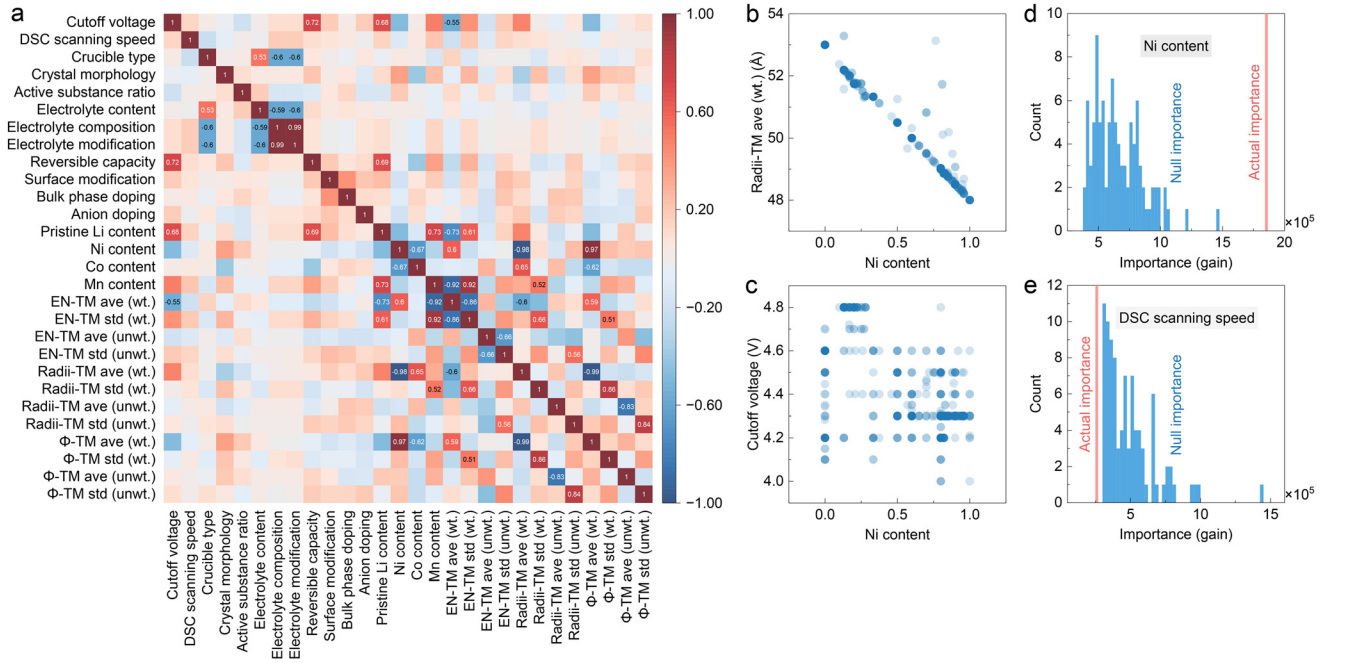

Fig. 1 The feature selection process. (a) Heatmap of Spearman correlation coefficients between all input features. (b) Relationship plot between the highly correlated Ni content and radii-TM ave. (wt.) features. (c) Relationship plot between the non-correlated Ni content and the cutoff voltage features. (d) Null importance distribution of the Ni content feature to the onset temperature output. (e) Null importance distribution of the DSC scanning speed feature to the onset temperature output.

monotonic line. This observation can be attributed to the smaller ionic radii of fully oxidized Ni^{4+} (0.48 Å) compared to Co^{4+} and Mn^{4+} (both 0.53 Å). Given that these three TM species dominate our dataset, the weighted average radii of TM are predominantly influenced by the stoichiometric ratio of Ni. In contrast, Fig. 1c demonstrates the uncorrelated relationship between Ni content and the cutoff voltage of the charged electrode sample for the DSC test. Following the principle of maintaining simpler and more fundamental features, we eliminated redundant variables based on a criterion of |Spearman coefficient| > 0.8. A detailed list of the features that have been eliminated is presented in the ESI.†

Further feature refinement was conducted using the null importance concept, which quantifies feature contribution to model performance when its relationship with the target is randomized.[28] For each target variable, we evaluated the actual gain importance of features using a random forest (RF) model implemented in the LightGBM package, subsequently generating 100 null importance values for each feature through independent shuffling. Fig. 1d illustrates the null importance distribution of Ni content in predicting heat release onset temperature. The significant decrease in importance post-shuffling demonstrates the feature's genuine relevance. Conversely, Fig. 1e shows that the actual importance of the DSC scanning speed does not exceed its null importance, indicating its irrelevance to the exothermic onset temperature. To maintain a comprehensive feature set for subsequent analysis, we employed a conservative screening strategy that excludes only those features whose actual importance is below the first quartile (25%) of the null importance values. The null importance feature screening approach aims to mitigate any interference that may hinder the precision of feature contribution analysis and model interpretation. It is important to note that this process was implemented independently for each target output variable, which may lead to divergent feature sets across various predictions. For instance, while DSC scanning temperature was excluded for onset temperature inference, it was preserved for maximum heat release power prediction. Detailed feature screening results are provided in the ESI.†

Model training

We employed the classical support vector regression (SVR) model for our analysis, a choice corroborated by recent literature as optimal for specific battery thermal runaway data analysis.[25] This selection was based on several considerations: SVR's exceptional ability to derive continuous outputs and identify outlier data points more effectively than simpler tree-based models; its suitability for small datasets, which reduces the risk of overfitting and enhances generalization compared to more complex models such as artificial neural networks (ANN); and importantly, its superior interpretability, which is essential for our feature contribution analysis. Fig. 2 illustrates the training and testing results for three target output variables that characterize the thermochemical reaction behavior of cathode materials: the onset temperature of the first apparent heat release peak, the temperature at maximum heat release power (peak temperature), and the maximum heat release power during the entire thermochemical reaction

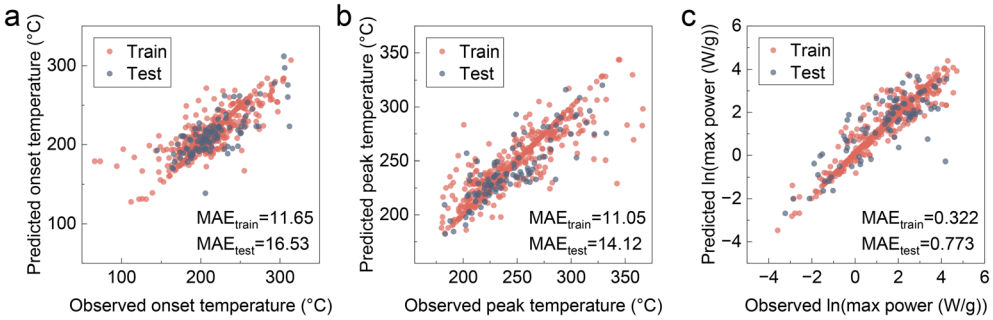

Fig. 2 Training and testing results of the selected features for the target thermochemical characteristic outputs of (a) onset temperature, (b) peak temperature, and (c) max power.

process (max power). The max power variable was logarithmically transformed to achieve a more balanced data distribution for improved regression. The model demonstrates robust performance across all three targets, with the majority of training and testing data points aligning along the diagonal. Although some outliers are presented, their influence on the general trends is considered negligible, given the inherent variability associated with experimental data.

Predictions in the elemental composition space

We validated our trained models by predicting the thermal behavior of NCM ternary materials charged to 4.3 V across varying elemental compositions. Virtual data points were generated by traversing the full NCM elemental composition space while maintaining consistent sample conditions and DSC testing parameters. The results are presented as ternary contour plots in Fig. 3a–c.

Fig. 3a illustrates that compositions with balanced stoichiometric ratios of the three TM species exhibit elevated onset temperatures, indicating delayed thermal reactions. This aligns with the reported excellent thermal stability of $LiNi_{1/3}Co_{1/3}Mn_{1/3}O_2$.[8] Conversely, mono-TM materials located at the triangle vertices ($LiCoO_2$, $LiMnO_2$, and$LiNiO_2$) display relatively low onset temperatures, suggesting inferior thermal safety. Notably, the high-Ni region exhibits very low onset temperatures, reinforcing the prevailing understanding of the significant thermal safety challenges associated with high-Ni NCM ternary materials despite their elevated reversible capacity. It is worth noting that while an increased Mn content typically enhances structural and thermal stability, this trend does not apply in extreme cases such as $LiMnO_2$, which has been reported to experience severe phase transition and oxygen release during cycling.[29] Peak temperature predictions (Fig. 3b) mirror onset temperature trends, with Ni content exerting a more dominant influence. The composition corresponding to the highest peak temperature shifts towards lower Ni content, suggesting that high Ni content not only triggers early onset but also accelerates the thermal reaction process. Intriguingly, the predicted maximum heat release power map (Fig. 3c) diverges from the previous two. While the high Ni vertex remains the most thermally active, the high-Mn area exhibits the lowest power, indicating a suppression of reaction severity. We attribute this phenomenon to the spinel phase transition process occurring in Mn-rich materials during thermochemical reactions, which results in a delayed concentrated heat release.[30] In summary, our analysis verifies the critical influence of Ni content on all three thermochemical characteristics, underscoring its significance in material thermal behaviors.

To validate our predictions, we juxtaposed our results against experimental data from two independent studies[31,32] that were not incorporated into our training or testing datasets. We emulated the sample conditions and DSC testing parameters from these works, adjusting solely the nickel content to align with their experimental design. The charging cutoff voltages in these studies were 4.3 V and 4.4 V, respectively. Our predicted onset (Fig. 3d) and peak (Fig. 3e) temperatures exhibited a strong correlation with the observed values. However, significant discrepancies were noted in the maximum power predictions (Fig. 3f). We hypothesize that the significant discrepancies between the predicted and reported maximum power values may be attributed to the high sensitivity of heat release power to external factors, such as the use of a not hermetically sealed crucible during DSC measurements and the incorporation of unknown additives in the electrolytes. This hypothesis is substantiated by the feature significance analysis results discussed in the subsequent sections of this paper. Given the complexity of these external factors, which are often inadequately detailed in the literature, it is possible that we have overlooked certain experimental or sample preparation conditions that could influence the DSC test results. Nonetheless, we contend that under consistent sample and testing conditions, the observed variation trends in our predictions still yield valid insights into the thermal behavior of the materials, as evidenced in Fig. 3f.

Explanation of feature impacts

To thoroughly investigate the influence of various features on thermochemical characteristics, we employed an explainable ML method on our trained models. The SHapley Additive exPlanations (SHAP) framework is widely recognized for its efficacy in interpreting ML model outputs. Recent studies have

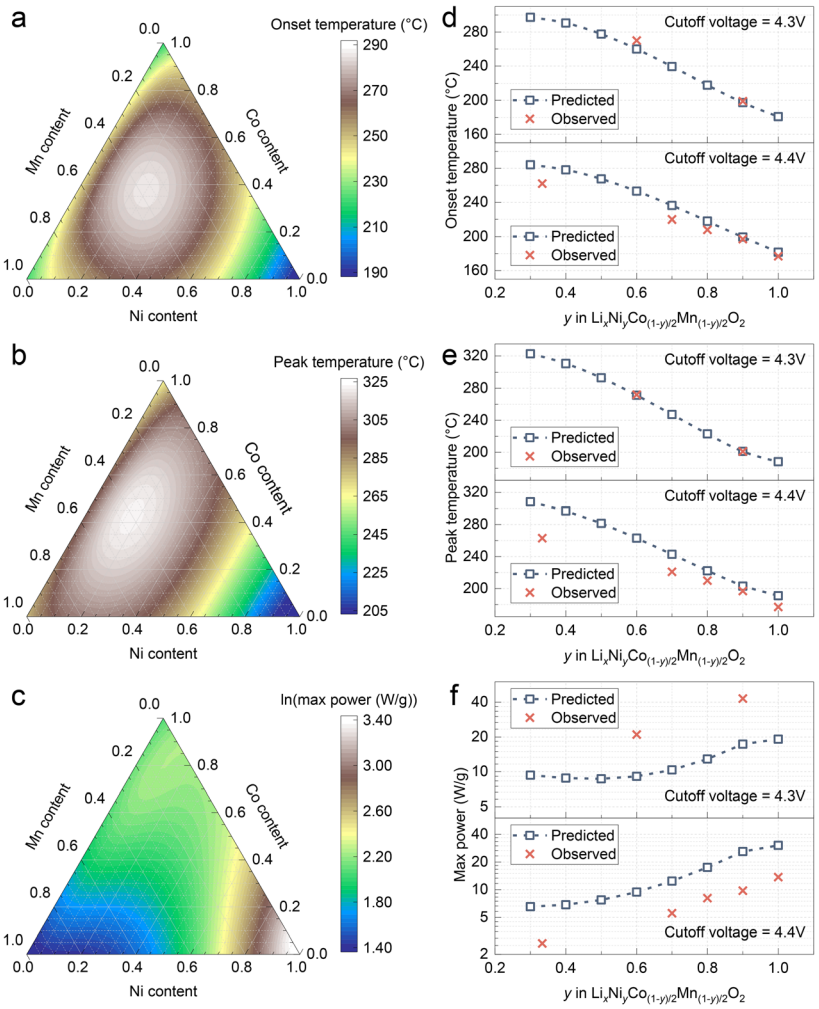

Fig. 3 Full NCM ternary space predictions for thermochemical characteristics of (a) onset temperature, (b) peak temperature, and (c) max power. Comparisons between the predicted and literature-observed evolution of (d) onset temperature, (e) peak temperature, and (f) max power to NCM material composition variations.

utilized SHAP to elucidate the relationships between particle geometries and degradation,[33] cathode material conditions and electrochemical performance,[18] cell metadata and thermal behavior,[25] formation parameters and battery cycling life,[14] electrolyte molecular structures and properties,[34,35] *etc*. We present the comprehensive summary plots of feature SHAP values in Fig. 4a–c. In these plots, the *x*-axis represents the standardized feature value, while the color of each data point indicates its influence on the model output. Notably, our findings reaffirm previous conclusions regarding material compositions. Higher Ni content correlates with negative contributions to onset and peak temperatures (Fig. 4a and b) and positive contributions to maximum power. A similar trend is observed for the Li content, which was not included in the composition analysis in Fig. 3. This relationship can be attributed to the increased thermal safety risk associated with oxygen release due to activated anion redox in an extensively delithiated sample.[36–38] Conversely, the feature radii-TM std (wt.), which quantifies the diversity of transition metal (TM) radii within the lattice, appears to have an opposing effect on thermochemical characteristics. The SHAP value distributions indicate that greater diversity in TM radii corresponds to higher onset and peak temperatures, as well as reduced heat release power. This phenomenon may be explained by the hindrance of TM migration during cycling due to larger differences between TM cation species, thereby enhancing overall structural stability.[39]

The influences of features related to material properties are consistently observed across all three thermochemical characteristics, while the impacts of features associated with sample preparation and DSC testing conditions may vary. We compared the SHAP value distributions of several representative features, as illustrated in Fig. 4d–g. The most significant DSC testing parameter affecting onset and peak temperatures is the cutoff voltage to which the samples were charged. Higher cutoff voltages negatively impact both characteristic temperatures, aligning with the understanding that highly oxidized cathode materials are more reactive in thermal contexts. However, this influence diminishes for maximum power, as

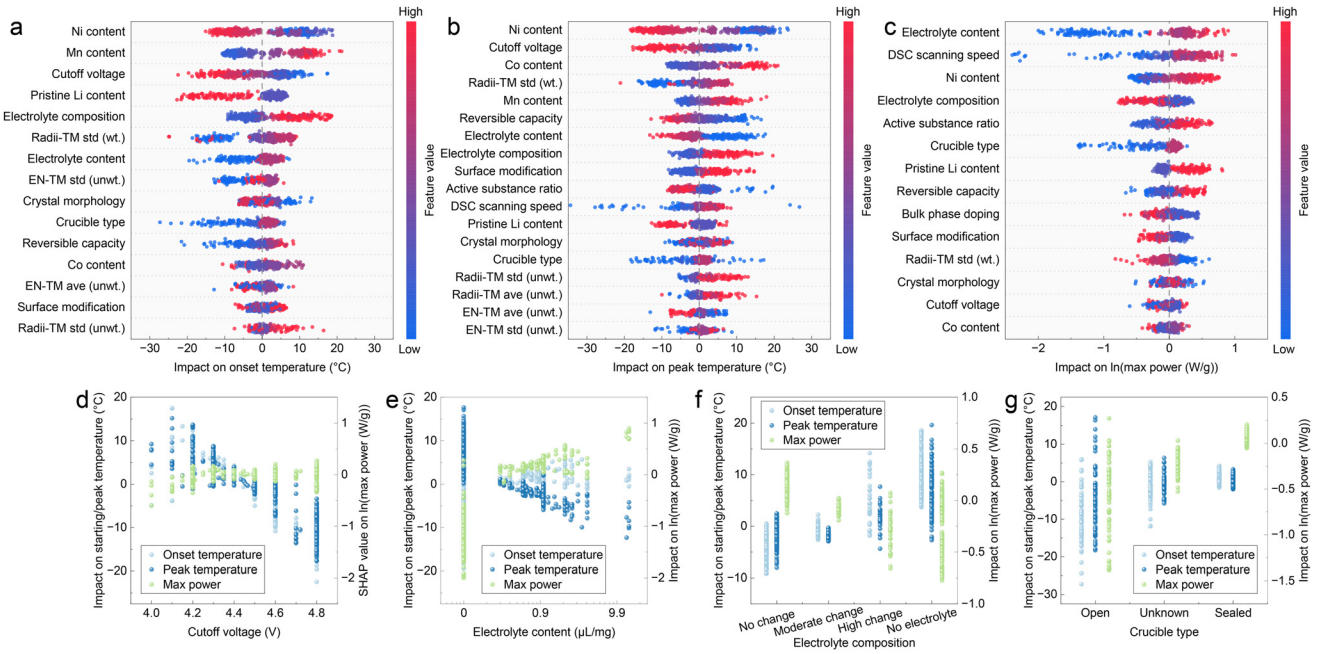

Fig. 4 Feature SHAP value distributions on the prediction of (a) onset temperature, (b) peak temperature, and (c) max power. SHAP value distribution variations upon the change of target output characteristics for features such as (d) cutoff voltage, (e) electrolyte content, (f) electrolyte composition, and (g) crucible type.

indicated by the SHAP value distribution showing no significant variation across different cutoff voltages (Fig. 4d), which we will address later.

Anomalous behavior is noted concerning the electrolyte content added during the DSC test. As shown in Fig. 4e, increased electrolyte content leads to earlier peak temperatures and higher power, likely due to the flammability of organic components in electrolytes. Conversely, the presence of electrolytes is anticipated to postpone the onset of thermochemical reactions, potentially explained by pre-reactions occurring between the electrolytes and cathode materials, which may safeguard the cathode from interacting with the electrolytes. Such moderate reactions may not produce prominent thermal release peaks in DSC results but can prolong the reaction and defer the heat release peak. Moreover, modifications in electrolyte composition significantly influence the thermal behavior of cathode materials. Fig. 4f indicates that electrolyte additives enhance battery thermal performance by increasing onset and peak temperatures while reducing heat release power, even though these additives primarily aim to improve electrochemical performance rather than thermal safety. We propose that improved thermal safety is a favorable byproduct of the enhanced stability of high-voltage interfaces achieved through the incorporation of electrolyte additives. Lastly, the type of crucible used in the DSC test is relevant; as shown in Fig. 4g, a sealed crucible is generally correlated with higher onset and peak temperatures, as well as increased instantaneous heat release power when compared to an open crucible.

It is important to note that SHAP values elucidate the relationships between input features and output characteristics; however, these correlations do not necessarily indicate causation. In the case of the crucible type, the observed correlation with maximum heat release power conflicts with the reported experimental phenomenon that thermal reactions proceed more gently under sealed systems,[40] therefore lacking a clear physical explanation. This issue can be approached from a data-driven perspective. Sealed crucibles used in DSC tests typically prevent the volatilization of electrolytes, creating an underlying collinearity with electrolyte content. The presence of electrolytes significantly enhances reaction intensity, thus linking closed crucibles to higher heat release power. This underscores the necessity of feature screening prior to regression analysis. Nevertheless, we cannot assure that all influential factors have been comprehensively considered or adequately described in the existing literature. Therefore, we cautiously ascribe SHAP value distributions that exhibit no clear trends to experimental data noise rather than making arbitrary conclusions.

Feature significance dynamics

We summarize the variance in feature influences across the three thermochemical characteristics, which correspond to the initiation, progression, and peak of a thermal runaway process. We calculated the mean absolute SHAP values for each feature associated with these characteristics and illustrated their variations in Fig. 5. To enhance clarity, we have included only the top five significant features for each thermochemical characteristic. The red-colored features, specifically Ni content, Mn content, and cutoff voltage, exert substantial influence on the first two characteristics, whereas their impact

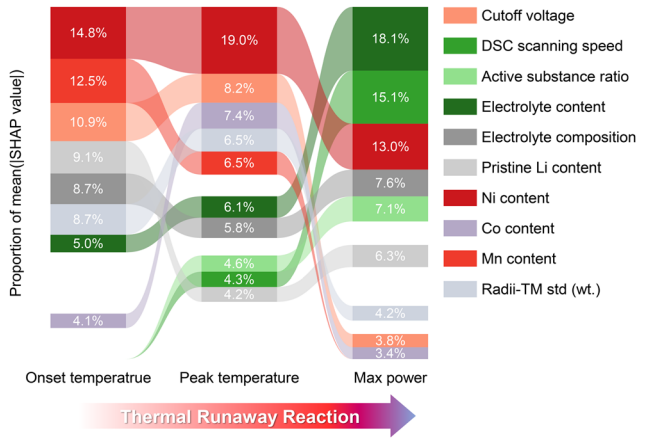

Fig. 5 Variation trends of feature significance to thermochemical characteristics corresponding to different stages of the thermal runaway reaction.

diminishes for heat release power. These are classified as "red-colored features". Conversely, the electrolyte content, DSC scanning speed, and active substance ratio show a marked increase in significance from onset and peak temperatures to maximum power and are classified as "green-colored features". Features without clear monotonic trends are categorized as "grey-colored features".

Upon a detailed examination of the red-colored features, we note that they are all related to material properties. Although the cutoff voltage is primarily regarded as a parameter in DSC testing, herein, it plays a crucial role in determining the actual lithium content within the delithiated material and influences the oxidation states of transition metal cations.[41] In contrast, the green-colored features pertain to sample conditions and DSC testing parameters. Notwithstanding the constraints posed by data scarcity and fidelity, we successfully delineated a fundamental understanding of the thermochemical reaction process of the layered oxide cathode materials. Specifically, the initial phases of the thermochemical reaction are predominantly governed by intrinsic material properties, while external conditions progressively dictate the dynamics of the reaction as it evolves. This understanding highlights the critical importance of managing various factors at distinct stages of the thermochemical reaction process. The conclusion also implies the need for a multifaceted approach towards thermal safety and considerations for optimizing materials.

Conclusion

In summary, we have developed a comprehensive thermochemical database for LIB cathode materials by compiling DSC testing results from the existing literature. Through the application of explainable ML, we conducted a systematic analysis of the complex interrelationships between thermochemical characteristics and their influencing factors. We have identified the intrinsic physical and chemical properties that dictate the thermal stability of cathode materials, as well as elucidated the external factors that affect the kinetics of thermochemical reactions. The trained SVR models confirm the significant influence of Ni content within the ternary composition space on material thermal behavior. A detailed analysis of SHAP values reveals consistent impacts of material properties on thermochemical characteristics, whereas the impacts of sample conditions and DSC testing parameters demonstrate greater variability. Furthermore, our investigation into feature dynamics throughout the thermochemical reaction process indicates a transition in dominant influences from intrinsic material properties to external conditions. These findings suggest that for the design of batteries exhibiting optimal thermal performance, it is essential to systematically investigate the reaction processes and optimize critical factors at each distinct stage of the reaction. Our work also demonstrates the effectiveness of data-driven ML methodologies in revealing fundamental patterns within extensive unstructured experimental datasets. Given the persistent challenges associated with data scarcity and fidelity, we aspire for our findings to advance the standardization of battery thermal analysis protocols and facilitate the creation of comprehensive experimental databases.

Author contributions

Yujian Sun: conceptualization, formal analysis, investigation, validation, visualization, and writing – original draft. Xilin Xu: conceptualization, data curation, investigation, and validation. Luyu Gan: investigation, validation, and writing – review & editing. Sichen Jiao: investigation and validation. Shuangshuang Han: data curation. Yajun Zhao: supervision. Yan Li: supervision. Xiqian Yu: conceptualization, writing – review & editing, funding acquisition, and supervision. Jizhou Li: investigation, methodology, validation, and writing – review & editing. Hong Li: funding acquisition and supervision. Xuejie Huang: funding acquisition and supervision.

Data availability

The data supporting this article have been included as part of the ESI.†

Conflicts of interest

There are no conflicts to declare.

Acknowledgements

This work is supported by the National Key R&D Program of China (2021YFB2500300) and the National Natural Science Foundation of China (Grant No. 52303301, 52325207 and 22239003).

References

1 A. Yoshino, *Angew. Chem., Int. Ed.*, 2012, **51**, 5798–5800.
2 J.-M. Tarascon and M. Armand, *Nature*, 2001, **414**, 359–367.
3 H. Maleki, G. Deng, A. Anani and J. Howard, *J. Electrochem. Soc.*, 1999, **146**, 3224.
4 X. Feng, M. Ouyang, X. Liu, L. Lu, Y. Xia and X. He, *Energy Storage Mater.*, 2018, **10**, 246–267.
5 Q. Wang, P. Ping, X. Zhao, G. Chu, J. Sun and C. Chen, *J. Power Sources*, 2012, **208**, 210–224.
6 S. Zheng, L. Wang, X. Feng and X. He, *J. Power Sources*, 2018, **378**, 527–536.
7 S.-M. Bak, E. Hu, Y. Zhou, X. Yu, S. D. Senanayake, S.-J. Cho, K.-B. Kim, K. Y. Chung, X.-Q. Yang and K.-W. Nam, *ACS Appl. Mater. Interfaces*, 2014, **6**, 22594–22601.
8 H.-J. Noh, S. Youn, C. S. Yoon and Y.-K. Sun, *J. Power Sources*, 2013, **233**, 121–130.
9 X. Xu, L. Gan, R. Chen, J. Wang, Z. Cai, X. Yu, H. Li and X. Huang, *Appl. Phys. Lett.*, 2024, **124**, 043901.
10 T. Kim, H. Chang, G. Song, S. Lee, K. Kim, S. Lee, J. Moon and K. T. Lee, *Adv. Funct. Mater.*, 2024, **34**, 2404806.
11 S. Korneev, H. Arunachalam, S. Onori and I. Battiato, *Transp. Porous Media*, 2020, **134**, 173–194.
12 X. Chen, X. Liu, X. Shen and Q. Zhang, *Angew. Chem.*, 2021, **133**, 24558–24570.
13 J.-N. Liu, C.-X. Zhao, J. Wang, X.-Q. Fang, C.-X. Bi, B.-Q. Li and Q. Zhang, *Joule*, 2024, **8**, 1804–1819.
14 X. Cui, S. D. Kang, S. Wang, J. A. Rose, H. Lian, A. Geslin, S. B. Torrisi, M. Z. Bazant, S. Sun and W. C. Chueh, *Joule*, 2024, **8**(11), 3072–3087.
15 X. Feng, H. Sha, Y. Zhang, Y. Su, S. Liu, Y. Jiang, S. Hou, S. Han and X. Ji, *Nat. Comput. Sci.*, 2024, 1–12.
16 Y. Wang, X. Feng, D. Guo, H. Hsu, J. Hou, F. Zhang, C. Xu, X. Chen, L. Wang, Q. Zhang, *et al.*, *Joule*, 2024, **8**, 2639–2651.
17 B. Bole, C. S. Kulkarni and M. Daigle, Annual Conference of the PHM Society, 2014.
18 A. Tsuchimoto, M. Okubo and A. Yamada, *Electrochemistry*, 2023, **91**, 037007–037007.
19 P. Zhong, B. Deng, T. He, Z. Lun and G. Ceder, *Joule*, 2024, **8**, 1837–1854.
20 R. Aversa, M. H. Modarres, S. Cozzini, R. Ciancio and A. Chiusole, *Sci. Data*, 2018, **5**, 1–10.
21 G. H. Carey and J. Dahn, *ACS Comb. Sci.*, 2011, **13**, 186–189.
22 C. R. Brown, E. McCalla, C. Watson and J. Dahn, *ACS Comb. Sci.*, 2015, **17**, 381–391.
23 H. M. Barkholtz, A. Fresquez, B. R. Chalamala and S. R. Ferreira, *J. Electrochem. Soc.*, 2017, **164**, A2697.
24 C. Ling, *npj Comput. Mater.*, 2022, **8**, 33.
25 K. Masalkovaitė, P. Gasper and D. P. Finegan, *Nat. Commun.*, 2024, **15**, 8399.
26 C. Spearman, *Am. J. Psychol.*, 1904, **15**, 72–101.
27 J. C. De Winter, S. D. Gosling and J. Potter, *Psychol. Methods*, 2016, **21**, 273.
28 A. Altmann, L. Toloşi, O. Sander and T. Lengauer, *Bioinformatics*, 2010, **26**, 1340–1347.
29 J. Ma, T. Liu, J. Ma, C. Zhang and J. Yang, *Adv. Sci.*, 2024, **11**, 2304938.
30 H. Pan, S. Jiao, Z. Xue, J. Zhang, X. Xu, L. Gan, Q. Li, Y. Liu, X. Yu, H. Li, *et al.*, *Adv. Energy Mater.*, 2023, **13**, 2203989.
31 H.-H. Sun and A. Manthiram, *Chem. Mater.*, 2017, **29**, 8486–8493.
32 Z. Cui and A. Manthiram, *Angew. Chem., Int. Ed.*, 2023, **62**, e202307243.
33 J. Li, N. Sharma, Z. Jiang, Y. Yang, F. Monaco, Z. Xu, D. Hou, D. Ratner, P. Pianetta, P. Cloetens, *et al.*, *Science*, 2022, **376**, 517–521.
34 Y.-C. Gao, N. Yao, X. Chen, L. Yu, R. Zhang and Q. Zhang, *J. Am. Chem. Soc.*, 2023, **145**, 23764–23770.
35 Y.-C. Gao, Y.-H. Yuan, S. Huang, N. Yao, L. Yu, Y.-P. Chen, Q. Zhang and X. Chen, *Angew. Chem., Int. Ed.*, 2024, e202416506.
36 M. Sathiya, G. Rousse, K. Ramesha, C. Laisa, H. Vezin, M. T. Sougrati, M.-L. Doublet, D. Foix, D. Gonbeau, W. Walker, *et al.*, *Nat. Mater.*, 2013, **12**, 827–835.
37 H. Yu, Y.-G. So, Y. Ren, T. Wu, G. Guo, R. Xiao, J. Lu, H. Li, Y. Yang, H. Zhou, *et al.*, *J. Am. Chem. Soc.*, 2018, **140**, 15279–15289.
38 S. Sharifi-Asl, J. Lu, K. Amine and R. Shahbazian-Yassar, *Adv. Energy Mater.*, 2019, **9**, 1900551.
39 J. Zheng, Y. Ye, T. Liu, Y. Xiao, C. Wang, F. Wang and F. Pan, *Acc. Chem. Res.*, 2019, **52**, 2201–2209.
40 S. Lee, K. Scanlan, S. Reed and A. Manthiram, *Adv. Energy Mater.*, 2024, 2403002.
41 A. Jain, G. Hautier, S. P. Ong, S. Dacek and G. Ceder, *Phys. Chem. Chem. Phys.*, 2015, **17**, 5942–5953.